Postprint of: Sosnowska A., Laux E., Keppner H., Puzyn T., Bobrowski M., Relatively high-Seebeck thermoelectric cells containing ionic liquids supplemented by cobalt redox couple, Journal of Molecular Liquids, Vol. 316 (2020), 113871, DOI: 10.1016/j.molliq.2020.113871

Relatively high-Seebeck thermoelectric cells containing ionic liquids supplemented by cobalt redox couple

Keywords:
Thermo-electricity, Seebeck coefficient, Galvanic cel, Ionic liquid, Redox couple, QSPR

Abstract:
Meanwhile no general and reliable equation determining the Seebeck coefficient (Se) and involving electrochemical reaction effects was derived for solutions. We reported the database of 15,000 ionic liquids supplemented by three different redox couple systems: 0.01 mol/l $Co^{3+/2+}$ $(bpy)_3$, 0.01 mol/l $I_3^-/3I^-$ and 0.2 mol/l $I_3^-/3I^-$, and the corresponding estimated Seebeck coefficients. We also reported methods for estimating Seebeck coefficients for those systems. First, Seebeck coefficients were measured for 17 ionic liquids and the 3 redox couples independently, and afterwards an analytical QSPR equationwas derived afterwhich the Seebeck coefficients for all possible combinations of cations and anions (resulting in 15,000 conceivable ionic liquid compounds)were derived. Following this, we analyzed the data and discovered tendencies and regularities. It was revealed that small, symmetrical and not branched cations and anions which contained less electronegative atoms, made the Seebeck increased. The highest Se = 2.3 mV/K, was observed for small ammonium and phosphonium cations with a triethyl-n-hexylboride anion. We also discovered that for thermo-electric applications cobalt-based redox couples are much better than the ones based on the iodine/iodide system.

1. Introduction

World energy consumption reached 14,000 Mtoe (million tons oil equivalent) in 2018, including coal, renewables, hydroelectricity, nuclear, natural gas, oil and in the same year global energy consumption increased by 2.9% [1,2]. This growth has been the strongest since 2010 and almost double the 10-years' average [1]. Moreover, carbon emissions grew by 2.0%, which was the fastest growth in seven years, and it seems the inter-governmental regulation policies such as Electronic Vehicles Initiative or the Paris Agreement (mandatory CO_2 gas emission reduction targets) have not changed the overall situation. Meanwhile, much of the consumed energy is lost to waste heat due to all levels of human activity. Thermal loss consists in several dozen percentage of the total energy consumption across different industrial sectors [1–3], and the situation is even worse in current applications of internal combustion and diesel engines where as much as from 60 up to 70% of the energy created is wasted as the heat emitted. Hence, if even a small fraction of waste-heat could be converted into more useful forms of energy (electrical, mechanical), it would result in tremendous savings to global energy consumption. It is known that the heat recovery can be practically accomplished in the Peltier device where the temperature gradient is utilized to achieve some amount of potential difference between the junctions and in turn - the electrical current and power. Two unique semiconductors, one n-type and one p-type, are used because they need to have different electron densities. The semiconductors are placed thermally in parallel to each other and electrically in series and then joined with a thermally conducting plate on each side. Currently, Peltier systems are commonly used i.a. in RTGs (radioisotope thermoelectric generators) that are used in satellites and space probes as the source of power. One of the leading examples for such application is the Voyager 1 probe sent by NASA into space on September 5th, 1977, still investigating Earth's Solar System and even beyond the heliosphere until today, while it is estimated that the nuclear fissile material used as the source of heat will allow for the operation of this probe until 2025. Similarly, other probes and spaceships are supplied in electrical energy thanks to Peltier systems. The most popular of them include the Cassini-Huygens probe or Apollo 12–17 spaceships.

The problem with the traditionally used thermoelectric materials is their efficiency, typically measured by the Seebeck coefficient which determines the open-circuit voltage (ΔV) produced by a device at any given temperature difference (ΔT): $S_e = -\Delta V/\Delta T$. The currently known semiconductor available on the market, best for such applications, is the bismuth telluride (Bi_2Te_3) for which the Seebeck coeff. amounts to 287 μV/K at 54 °C [4]. This material is in addition toxic and expensive. Actually, solid semiconductors achieved their upper limit in

thermoelectric conversion several years ago, while the development remains minor. Fortunately, there are other possibilities. Recently, it has been demonstrated that ionic liquids supplemented by appropriate redox couple could play a role similar to that of the bismuth telluride semiconductor in 'traditional' thermoelectric devices [4,24,27,28]. Liquid thermoelectric cells may have a small diameter (one or a few millimeters) and can be placed in a polymeric matrix (flexible and e.g. transparent) or a ceramic one (non-flexible yet resistant to higher temperatures), see Fig. 1.

Ionic liquids are typically characterized by the melting point lower than 100 °C, but obviously there are known ionic liquids which melt in higher or in lower temperatures. Ionic liquids are salts in liquid state and are largely made of ions and short-lived ion pairs. Structurally they are most frequently composed of an asymmetrical cation and an anion which often includes a non-metal ion. Due to the characteristics of high chemical stability and the recycling opportunity, ionic liquids are becoming more and more popular in industrial applications [5,6]. Ionic liuqids in room temperature possess distinctively high ionic conductivity, nearly zero vapor pressure, and inflammability, which makes them an attractive new-type of solvent [7–11]. Due to their strict ionic nature, which is typical for crystals, they expose specific molecular and physical peculiarities including engagement in catalytic reactions and in electrochemical processes [12–15]. But ILs are liquid, and anions and cations are mobile, which makes the resulting dipole moment different than for normal polar solvents. Moreover, due to high viscosity and presence of polar and non-polar structure's fragments, the mesoscopic organization of ionic liquids is heterogeneous [16–19]. By changing a cation or an anion, an ionic liquid, therefore such that has other physical and chemical characteristics. Hence, the key to the application of ionic liquids i.a. in the thermo-electric conversion might consist in proper selection of ions of such liquid [20,21]. The number of possible combinations of cations and anions has been estimated to amount to 10^{18} [22], thus any method thanks to which it would be possible to predict the characteristics of even hypothetically existing ionic liquids is very valuable.

Moreover, the neat ionic liquids display thermo-electric qualities themselves; Seebeck coefficients measured for neat ionic liquids are relatively large, reaching 1.44 mV/K for [EMIM] [Tf_2N] [23]. This is interesting because ionic liquids are typically supplemented in thermo-electric cells by the so-called redox systems, therefore such that, as it is assumed, fulfill a role similar to solvents with electrolytes dissolved there. It is commonly believed that ions in redox pairs actively participate in reduction on a cathode and oxidation on an anode, and that the difference in potentials between the two electrodes is created as a result of thermal expansion of ions between electrodes (thermal diffusion), however also in relation to other facts (non-published) it would seem that the conduction mechanism in such systems is much more complex and might take redox reactions in the whole system into consideration. Jia and coworkers dissolved ILs in water and achieved both p-type and n-type thermoelectric materials [24].

It should be noted that not only ionic liquid-based liquid thermocells have been tested so far. Bonetti and coworkers proved that the 0.1 M of lipophilic salt, tetrabutylammonium nitrate, in 1-dodecanol, exposed the Seebeck coefficient equal to even 7 mV/K [25]. In addition, it has recently been shown that the suspension of respectively selected ferromagnetic nanoparticles included in a respective organic solvent considerably increased the value of the Seebeck coefficient, which was believed to be (at least partially) related to the Sorret effect [26], not yet explored in total.

Laux and coworkers showed many laboratory results for ionic liquids containing the $I_3^-/3I^-$ redox couple, whereas the resulting Seeebeck coefficients were much higher than those found for the traditional Bi_2Te_3 semiconductor [4,27,28]. A systematic analysis of the influence of ionic liquids supplemented with the $I_3^-/3I^-$ redox couples on the Seebeck coefficient and on the viscosity in thermocells was done by Sosnowska et al. [10,31]. Al Masri and coworkers [30] revealed that four cobalt complexes soluted in a mixture of DMSO and the same ionic liquid display regularly higher Seebeck coefficients than in case of ionic liquids supplemented by the $I_3^-/3I^-$ redox couple [31]. High Seebeck for ionic liquids containing cobalt complexes was also found by He et al. [32]. Cobalt complexes and ionic liquids were used as dye-sensitized solar cells, where the cobalt complexes revealed to be an attractive alternate to the 'traditional' $I_3^-/3I^-$ redox shuttle [33].

The design of chemicals with desirable activity/property, supported by computational methods, was reported many times [34–39]. Ionic liquids, among other compounds, were successfully designed in a similar manner [29,38,40–45]. In current work, we determine structural features of ionic liquids' anions and cations that influence the value of the Seebeck coefficient in different redox couple systems. For this purpose, we took experimental values of Seebeck coefficients for ionic liquids supplemented by cobalt complexes and on this basis we developed the arithmetic Quantitative Structure-Property Relationship (QSPR) model to estimate the Seebeck for 15,000 ionic liquids. We also applied the previously developed QSPR model and estimated the Seebeck coefficients for the same 15,000 ionic liquids containing the $I_3^-/3I^-$ redox couple (0.2 mol/l concentration) [10]. We also worked out yet another QSPR model for ionic liquids supplemented by the 0.01 mol/l $I_3^-/3I^-$ redox couple system. At the end, we performed a thorough analysis between the two models and the two different thermo-electric systems.

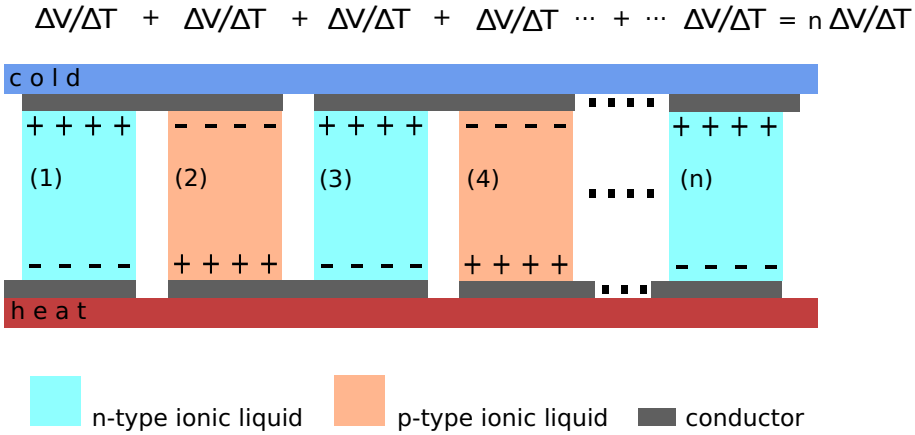

Fig. 1. Peltier-like schematic thermoelectric plate based on ionic liquids. The p-like and the n-like cells were linked with the conducting material. The n-type and the p-type pairs of ionic liquids are not always equally efficient.

2. Methods

2.1. Experimental measurements

2.1.1. Materials

The following 17 ionic liquids were used in a specially designed measurement set-up: IL1 - 1-ethyl-3-methylimidazolium tetrafluoroborate, IL2 - 1-butyl-1-methylpiperidinium bis(trifluoromethanesulfonyl)imide, IL3 - 1-ethyl-3-methylimidazolium trifluoromethanesulfonate, IL4 - 1-(2-Methoxyethyl)-1-methylpiperidinium bis(trifluoromethanesulfonyl) imide, IL5 - 1-methyl-1-(2-methoxyethyl)pyrrolidinium bis (trifluoromethylsulfonyl)imide, IL6 - 1-butyl-1-methylpyrrolidinium bis(trifluoromethylsulfonyl)imide, IL7 - H-ethylimidazolium bis (trifluoromethylsulfonyl)imide, IL8 - N-ethyl-*N*,*N*-dimethyl-N-(3-methoxypropyl)ammonium bis(trifluoromethanesulfonyl)imide, IL9 - SBMI bis(trifluoromethylsulfonyl)imide, IL10 - 1-butyl-3-methylimidazolium bis(trifluoromethylsulfonyl)imide, IL11 - 1-ethyl-3-methylimidazolium bis(fluorosulfonyl)imide, Il12 - 1-propanol-3-methylimidazolium bis(trifluoromethanesulfonyl)imide, IL13 - 1-ethyl-3-methylimidazolium bis(trifluoromethylsulfonyl) imide, IL14 - 1-(3-methoxypropyl)-3-methylimidazolium bis (trifluoromethanesulfonyl)imide, Il15 - *N*,*N*,*N*-trimethyl-N-butylammonium bis(trifluoromethanesulfonyl)imide, IL16 - butylammonium bis(trifluoromethanesulfonyl)imide, IL17 - 1-ethyl-3-methylimidazolium dicyanamide.

All ILs originated from SOLVIONIC SA (Toulouse, France). In each case, the total concentration of impurities was less than 2% and the ILs were used as obtained.

Cobalt complexes with pyridine chelating ligands - tris(2,2′-bipyridine) cobalt (III/II) [bis(trifluoromethane)sulfonimide]$_{2/3}$, further denoted as the $Co^{3+/2+}(bpy)_3$ $(TFSI)_{3/2}$ (or simply $Co^{3+/2+}$), were synthesized following the procedure reported by Abraham and coworkers [48].

Namely in the case of $[Co^{II}(bpy)_3][TFSI]_2$ first the salt of $Co(II)Cl_2$. 6H2O (8.4 mmol) and 2,2-bipyridyl (27.9 mmol) were dissolved in methanol. The solution refluxed for 2 h after which Lithium (trifluoromethansulfonyl)imide (20 mmol) was added. Solution was stirred and product precipitated out of solution. In the case of $[Co^{III}(bpy)_3][TFSI]_3$ first 1.2 mmol of $Co^{II}(bpy)_3(TFSI)_2$ was dissolved in acetonitrile after which the nitrosyl tetrafluoroborate (1.5 mmol) was added to the solution. Next the Lithium (trifluoromethansulfonyl) imide (6 mmol) was added and then the solution was stirred and product precipitated out of solution.

2.1.2. Thermocell Seebecks' measurements

The S_e coefficient measurement set-up used at HES-SO is shown in Fig. 2. It consisted of two thermally highly conductive sapphire plates that were coated with an inert electrode material (1 μm Rhodium) that was in contact with the liquid. One pair of contact finger measured the voltage drop between the adjacent rhodium electrodes exposed to T_{hot} and to T_{cold}, while the other pair was connected to a computer-controlled switch system allowing to measure open circuit potential or apply different load resistors (between 2 Ω and 100 MΩ) to current determination when used for a TEG characterization. To avoid IL losses, the cell was sealed using a silicone gasket (d = 4 mm). The aluminum bodies were connected with a heater (thermal resistor, Vitelec, France) and cooler system (Thermostat Frigiterm, J.P. Selecta S.A, Barcelona, Spain); the thermocouples (Type K, Jumo-Regulations, Metz, France) were placed close to the sapphire plates between the liquid and the heater, respectively cooler. The resistances between 5 Ω and 100 MΩ have a tolerance of 0.1%. Every 10 s a measurement was taken while maximum errors from the measurement system were less than 1 μV and ± 1.5 K.

The determination of the Seebeck coefficient was based on a linear dependency between the temperature and voltage and was used subsequently to determine the relative Seebeck coefficient. The electrode was heated up by means of a heating resistor, and every 10 s the temperature and voltage were registered. Maximum and minimum cell potentials, as well as maximum and minimum temperature differences between hot and cold electrodes were read out. We noticed that during the heating and cooling the correlation of some ILs was not linear. After two temperature cycles, the linear behavior was established for all ILs. For all measured Seebeck coefficients, the difference between the heating and cooling was less than 60 μV/K. The published values were taken from the cooling curves. The relative Seebeck coefficient was determined from the slope of the measured voltage-temperature curve by using the following equation: $S_e = (U_{max} - U_{min}) / (\Delta T_{max} - \Delta T_{min})$.

2.2. Theoretical study

2.2.1. Molecular descriptors

The molecular models of 17 ILs (each anion and each cation separately) were created by using the ChemSketch [46] software. Each structure of an ion (the total spin was equal to 0 in case of each ion while its net charge was equal to +1 or to −1) was first optimized by using the semi-empirical Parametric Method 7 (PM7) [47], as implemented in the MOPAC software [49]. The PM7 method was recently recommended for

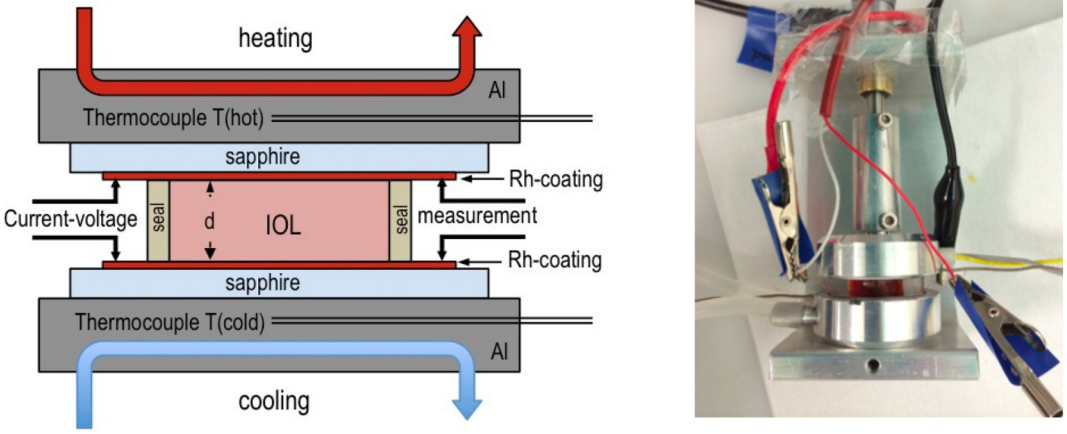

Fig. 2. Left panel - representation of setup thermocell, *right panel* - actual thermocell for operating temperatures of 200–250 °C.

Table 1
Experimental values of Seebeck coefficients ($S_{e\ exp}$) for corresponding ILs. Predicted values of the Seebeck coefficient ($S_{e\ p}$) were shown too. QSPR descriptors were collected in the following columns: MPC03_C and HATSs_A.

	Ionic liquid	MPC03_C	HATSs_A	T/V	$S_{e\ exp}$	$S_{e\ p}$	Std res	Lev
IL1	1-Ethyl-3-methylimidazolium tetrafluoroborate	2.485	576.000	1	1.314	1.276	−0.740	0.315
IL2	1-Butyl-1-methylpiperidinium bis(trifluoromethanesulfonyl)imide	2.773	415.074	1	1.370	1.431	1.521	0.135
IL3	1-Ethyl-3-methylimidazolium trifluoromethanesulfonate	2.485	459.850	2	1.384	1.417	0.841	0.110
IL4	1-(2-Methoxyethyl)-1-methylpiperidinium bis(trifluoromethanesulfonyl)imide	2.773	415.074	1	1.400	1.431	0.899	0.135
IL5	1-Methyl-1-(2-Methoxyethyl)pyrrolidinium bis(trifluoromethylsulfonyl)imide	2.708	415.074	1	1.401	1.440	1.049	0.117
IL6	1-Butyl-1-methylpyrrolidinium bis(trifluoromethylsulfonyl)imide	2.708	415.074	2	1.441	1.440	0.236	0.117
IL7	H-Ethylimidazolium bis(trifluoromethylsulfonyl)imide	2.303	415.074	1	1.446	1.497	1.248	0.092
IL8	N-Ethyl-*N*,*N*-dimethyl-N-(3-methoxypropyl)ammonium bis(trifluoromethanesulfonyl)imide	2.303	415.074	1	1.448	1.497	1.208	0.092
IL9	SBMI bis(trifluoromethylsulfonyl)imide	2.890	415.074	2	1.458	1.415	−0.522	0.176
IL10	1-Butyl-3-methylimidazolium bis(trifluoromethylsulfonyl)imide	2.639	415.074	1	1.466	1.450	−0.074	0.103
IL11	1-Ethyl-3-methylimidazolium bis(fluorosulfonyl)imide	2.485	428.814	1	1.475	1.455	−0.154	0.090
IL12	1-Propanol-3-methylimidazolium bis(trifluoromethanesulfonyl)imide	2.639	415.074	2	1.499	1.450	−0.633	0.103
IL13	1-Ethyl-3-methylimidazolium bis(trifluoromethylsulfonyl)imide	2.485	415.074	1	1.517	1.471	−0.650	0.086
IL14	1-(3-Methoxypropyl)-3-methylimidazolium bis(trifluoromethanesulfonyl)imide	2.708	415.074	1	1.529	1.440	−1.555	0.117
IL15	*N*,*N*,*N*-Trimethyl-N-butylammonium bis(trifluoromethanesulfonyl)imide	1.792	415.074	2	1.610	1.567	−0.517	0.269
IL16	Butylammonium bis(trifluoromethanesulfonyl)imide	1.099	415.074	1	1.667	1.664	−0.269	0.880
IL17	1-Ethyl-3-methylimidazolium dicyanamide	2.485	88.788	1	1.886	1.867	−1.889	0.837

$MPC03^C$ - molecular path count of order 3, and for anions – HATSsA - leverage weighted total index weighted by I-state, T/V - training/validation set, $S_{e\ exp}$ - measured Seebeck coefficient, S_p - predicted Seebeck coefficient, Std res - standardized residuals, Lev - leverage values.

the ionic liquids' geometry optimization because the QSPR correlation coefficients found for such structures were sufficiently high while the computing time (dedicated for the optimization) was low [41]. The optimized structures were in turn used for the calculation of molecular descriptors by means of the DRAGON software [50]. 3694 descriptors were calculated for each IL (2648 descriptors for each cation moiety and 1046 for each anion moiety).

2.2.2. QSPR modelling

The measured values of the Seebeck coefficient for 17 IL compounds supplemented by 0.01 mol/l concentration of the cobalt redox couple have been included in Table 1.

In the first step of the QSPR modelling, the data is split into sets used for calibrating (the training set) and for validating (the validation set) the model. The 17 ionic liquids were first sorted according to increasing S_e values. Next, every third compound was assigned to the validation set, whereas the remaining compounds formed the training set. The created training set contained 12 ILs (71% of all ILs studied), whereas the validation set - 5 compounds (29%), see Table 1.

In the next step we selected the most appropriate descriptors from among constitutional, structural, quantum chemical and other ones. There are thousands of descriptors available, while their choice for predicting distinct new structures of ionic liquids and the corresponding Seebeck coefficient must be pertinent. The optimal descriptors for modelling were selected by employing the Genetic Algorithm (GA) [51] as implemented in the QSARINS software [52,53]. The intuitive criteria were the highest validation and cross-validation parameters for the final QSPR model. The GA setup was as follows: generation per size = 500; mutation rate = 20%. Next, the Multiple Linear Regression (MLR) approach [54,55] was applied. The intrinsic assumption was that the equation representing the Seebeck coefficient might have a linear form, whereas the molecular descriptors represent independent variables. The model was next developed by using the QSARINS software [53,54]. The internal (leave-one-out (LOO) method) [56] and the external (with data not used for calibrating the model) validation of the developed model was performed, according to the OECD recommendations [57,58]. The evaluation of the goodness-of-fit, stability, robustness and limitations as well as the predictive ability of the developed model was performed by estimating the determination coefficient (R^2), squared cross-validation and external coefficients (Q^2), the root mean square errors of calibration, cross-validation, and external validation (RMSE), r^2_m metrics for internal, external and overall validation tests, concordance correlation coefficient (CCC), and the mean absolute error (MAE) [59–61]. The detailed criteria of estimated parameters are shown in Table 2 [61–64]. Additionally, to avoid bias in descriptors' selection, we applied the double cross-validation method [65]. Moreover, the dependent-variable randomization test (Y-scrambling) was applied for reducing the possibility of correlation-by-chance and for the confirmation of the statistical significance of the developed model [65–67]. The applicability domain of the developed model, which described the theoretical space limited by the structural/physicochemical properties of the chemicals from the training set, was defined using the leverage approach (the Williams plot) [68]. In this approach, the applicability domain is a square limited by the ±3 standard deviation units and the critical h* leverage value, ($h^* = 3p'/n$, where p′ is the number of model variables enlarged by one, and n stands for the number of compounds in the training set).

Table 2
QSPR models used for S_e prediction.

Redox couple	QSPR equation	Ref.
0.01 M $I_3^-/3I^-$	$S_{e\ QSPR1} = 0.413–0.1472piPC04^C + 0.26GATS1i^A$	[10]
0.2 M $I_3^-/3I^-$	$S_{e\ QSPR2} = 0.32–0.17piPC04^C + 0.15GATS1i^A$	Model presented in SI1
0.01 M $Co^{3+/2+}$	$S_{e\ QSPR3} = 1.493–0.063MPC03^C – 0.132HATSs^A$	This study

2.2.3. Seebeck coefficients for ILs supplemented by two different redox couple salts

The number of hypothetical structures of ionic liquids is tremendous [22]. On the other hand, there is also some amount of possible redox couple salts, whereas not each of them can be soluted in individual possible ionic liquid. In current work we worked out three independent QSPR models: two for cases of 0.01 M and of 0.2 M concentrations of the $I_3^-/3I^-$ redox couple in ILs and one for the case of 0.01 M concentration of the $Co^{3+/2+}(bpy)_3$ redox couple in ILs, see Table 2. The basis for these investigations were the experimental measurements of Seebeck coefficients for all three cases while the number of ILs taken into account in the measurements was equal to 20 in the case of 0.01 M concentration of the $I_3^-/3I^-$ redox couple and 17 in two other cases.

After the QSPR models were worked out and taught on how to work with ionic liquid compounds for each case of respective redox couple concentration, we constructed a virtual library of 15,000 IL compounds crossing the most popular 200 different cations and 75 different anions (for more details please refer to the Table S2.1 in SI2). In the case of each individual compound we optimized its structure as described above, and next for each optimized structure of an ionic liquid we calculated appropriate descriptors which were used alongside in the QSPR model for estimating Seebeck coefficients for the ILs supplemented by all three different concentrations of the redox couples. On the basis of this protocol we achieved Seebeck coefficients for 15,000 ILs for each redox couple and its specific concentration. At the end we compared the so obtained Seebecks mutually corresponding to appropriate ILs' structures and analyzed the relationships.

3. Results

At the beginning we measured Seebeck coefficients for 17 ionic liquid cells. The ionic liquids were supplemented by 0.01 mol/mol cobalt III/II redox couple, which, as it is believed, plays a role of the system of electron exchange occurring at electrodes (at least there). This in turn means that the ionic liquid would play a role of a solvent in this model, however the exact role of ionic liquid ions in thermoelectric or capacitor applications remains not thoroughly investigated. On the other hand, it is known that at least some neat ionic liquids display relatively high Seebeck [23]. The measurements or each system of ionic liquid and cobalt salt were done in the same manner, described more precisely in the experimental section. In the next step we optimized structures of ions of all ILs, and for each ion we calculated the descriptors. The application of the GA algorithm allowed for selecting two descriptors which were the most suitable for modelling the S_e. These descriptors were the following ones (adopting the QSAR naming standard): for cations - $MPC03^C$ – molecular path count of order 3, and for anions - HATSsA - leverage weighted total index weighted by I-state. The $MPC03^C$ descriptor is related to definite structure properties, while the $HATSs^A$ is related to electronegativity. A deeper analysis is done in the next chapter. The correlation coefficients of these descriptors for training and validation sets were lower than 0.024. Next, the Multiple Linear Regression approach was applied to finally derive the arithmetic QSPR equation (Eq.1) which brings the relationship between the structural features of the ILs and the Seebeck coefficient. The final equation is as follows:

$$\mathbf{S_e}^{Co3+/2+} = \mathbf{1.493}\ (\pm\mathbf{0.015}) - \mathbf{0.063}\ (\pm\mathbf{0.015})\ \mathbf{MPC03}^{\mathbf{C}} - 0.132\ (\pm 0.015)\ \mathbf{HATSs}^{\mathbf{A}} \quad (1)$$

where,

$MPC03^C$ – molecular path count of order 3, calculated for a given cation, $HATSs^{A-}$ leverage weighted total index/weighted by I-state, calculated for a given anion.

In order to review the quality of the developed QSPR equation, we calculated the goodness-of-fit, stability and robustness parameters, see Table 3 [52,59,60,63,64]. High, close to one and similar values of determination coefficients (R^2, Q^2_{CV}, Q^2_{EXT}, and CCC_{Ext}) and low, close to zero and similar to one another error values ($RMSE_C$, $RMSE_{CV}$, $RMSE_{EXT}$) point out that the developed model is well-fitted, robust and characterized by satisfactory predictive ability. Such statement can additionally be confirmed by the visual analysis of the observed vs. predicted values of the S_e, see Fig. 3, left panel. All points (from training and validation sets) were distributed near the solid line which indicated an ideal match of x to y values. However, one parameter calculated for developed model ($(r^2 - r_0'^2) / r^2$) had a higher then recommended value. This may suggest that the majority of the predicted values (from the validation set) were in fact lower than the ones observed. This result is also seen in the Fig. 3 - left panel where four out of five points from the validation set were located under the solid line. Nevertheless, this is an acceptable situation in the model because for smaller sets of data, the distribution of errors can simply occur by chance. Moreover, in order to avoid bias in the selection of descriptors, we performed the Double Cross-Validation analysis [65]. All statistical metrics estimated within internal and external validation steps (see Table S1.1) meet the cut-off criteria recommended by Roy et al. [61,65].

Table 3
Calculated parameters for internal and external validation of the QSPR model.

Measure [52,59,61,63,64]	Calibration	Cross-validation (loo)	External validation	Criteria [60,61,63,64]
F	44.28	–	–	Dependent[a]
R^2	0.908	–	–	> 0.7
Q^2	–	0.821	0.933	> 0.6
CCC	0.952	0.892	0.846	>0.85
RMSE	0.044	0.062	0.034	Acceptable[c]
MAE	0.034	0.05	0.034	Good[d]
average r^2_m	–	–	0.613	> 0.5
Δr^2_m	–	–	0.196	< 0.2
$(r^2 - r_0^2) / r^2$	–	–	0.033	< 0.1
$(r^2 - r_0^2) / r^2$	–	–	0.185	< 0.1
k	–	–	0.986	0.85 ≤ k ≤ 1.15
k'	–	–	1.004	0.85 ≤ k' ≤ 1.15
$\lvert r_0^2 - r'^2_0 \rvert$	–	–	0.13	< 0.3

[–] – measure does not refer to the procedure; a – F criterion is dependent on the number of compounds in the set, should be higher than tabulated value of F of chosen significance, b – value of the Q^2 parameter in the validation procedure refers to Q^2_{F3}; c – RMSE should be as low as possible and is estimated based on the range of response values of the training set; d – MAE, if possible (enough data points are available), is based on MAE-based metrics that are recommended by Roy et al.

In order to prove that the presented model is relevant and the lack of the so-called correlation-by-chance, we evaluated the statistical significance of the developed QSPR model by performing the 200-fold Y-randomization test (using two selected descriptors, $MPC03^C$ and $HATSs-^A$). The randomly generated models were characterized by two times higher $RMSE_C$ and $RMSE_{CV}$ values, see Fig. 3, right panel.

A good praxis is that the operating QSPR model gives reliable predictions of high probability within the well-defined structure space. This structure space is called the Applicability Domain (AD). For this purpose, we applied the leverage approach combined with the Williams plot, see Fig. 4. On the basis of this approach one can show the standardized residuals (differences between the observed and predicted Seebeck values) as a function of leverage values, which in turn indicates the similarity of particular compounds to the training set structures. The AD here is a square determined by three standard deviation units, 3σ, and the threshold value of leverage, h*. According to this approach almost all compounds belong to the AD of the developed model. Two compounds from the training set (IL16 and IL17) have the leverage, h, and values greater than the threshold h*, which means that the structure of these compounds significantly differs from training set structures. However, the predicted Seebeck coefficients are reliable and therefore the points are 'good leverages' and reinforce the derived QSPR model [69].

In general, the QSAR modelling leads to the mechanistic interpretation on the phenomenon of the property described, and the appropriate interpretation must be done on the basis of the analysis of particular descriptors selected for the model. In the case where the Seebeck coefficient is being sought, two descriptors were finally chosen as the ones which have had the greatest impact on the Seebeck coefficient. The first descriptor, MPC03C, i.e. the molecular path count of order 3, is calculated for cation moiety. Molecular path counts are molecular descriptors derived from the molecular graph, based on counting of paths. The length of paths, here equal to 3, denotes that three edges of the cation were involved in the path calculation. This descriptor provides useful information on the size, branching and the symmetry of a particular cation. The $MPC03^C$ shows large values when the molecular volume and branching increase. For example, the values of $MPC03^C$ are higher for the 1-butyl-3-methylimidazolium and the *N*,*N*,*N*-trimethyl-N-butylammonium than for the 1-ethyl-3-methylimidazolium

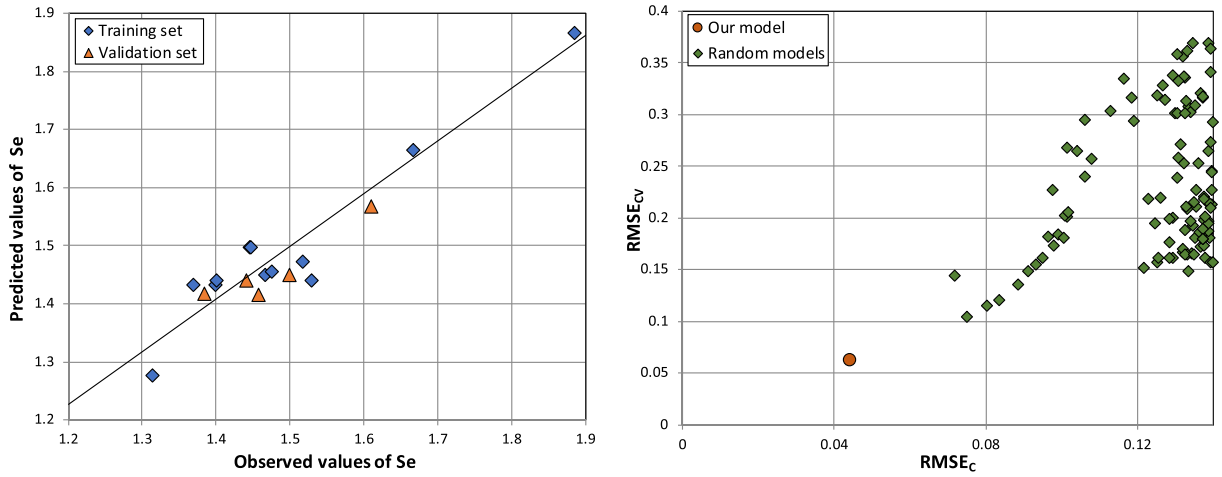

Fig. 3. Left panel – observed vs. predicted values of Se, right panel – Y–randomization plot.

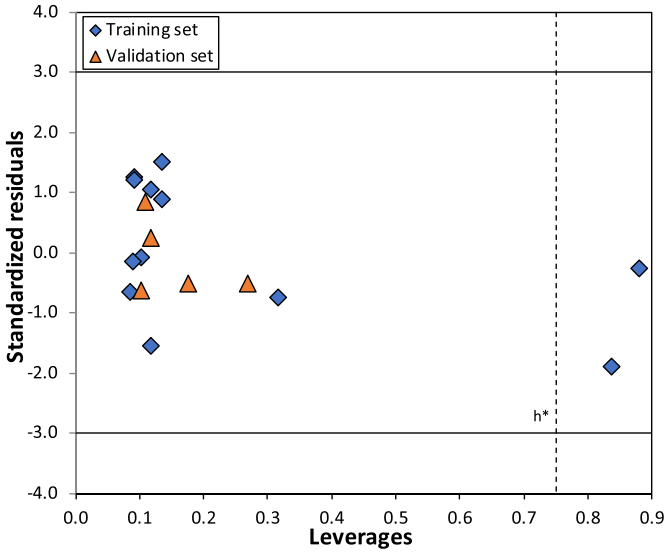

Fig. 4. Williams plot: standardized residuals versus leverages. Solid lines indicate ±3 standard deviation units, dashed lines indicate the threshold value (h* = 0.75).

and butylammonium respectively, see Table 4. The former two cations are larger and more branched.

The second descriptor, HATSs^{A} (leverage weighted total index/weighted by I-state, calculated for anion) comes from the H-GETAWAY class of descriptors calculated based on the molecular influence, **H** matrix: $\mathbf{H} = \mathbf{M} \times (\mathbf{M}^{T} \times \mathbf{M})^{-1} \times \mathbf{M}^{T}$. The molecular matrix, **M**, is calculated based on the centered Cartesian coordinate of a molecule (with hydrogens included), for their optimized geometry. The HATS indices are a class of structural, 3-dimensional descriptors determined by weighting each atom of a molecule by its various properties and combined with diagonal elements of the molecular influence **H matrix**. This class of descriptors encodes information about the impact of particular atoms/fragments on a molecule's shape and size, as well as on specific atomic properties. The atoms in GETAWAY descriptors can be weighted by: atomic mass, polarizability, ionic potential, van der Waals volume and electronegativity [70]. The HATSs total index is defined as a sum of all the HATS indices weighted by the so called intrinsic stage (I-stage, s):

$$HATSs = HATS_0 s + 2 \times \sum_{k=1}^{D} \hat{S}_k s.$$

where D is the maximum topological distance in a molecule and k is the maximum number of atoms in a molecule used for calculating the distance.

The weighted scheme - intrinsic stage - is derived from the ratio of the Kier-Hall electronegativity to the number of skeletal sigma bonds for each atom. Therefore, for less electronegative atoms present in anion structures, the I-stage remains relatively small and increases for more-electronegative atoms, especially for those containing few skeletal connections [71]. We noticed that anions containing highly electronegative atoms displayed relatively higher HATSs^{A} descriptor values, see Table 5.

The signs of the equation coefficients related to both descriptors in the QSPR model are negative, which means they are inversely proportional to Seebeck coefficient values; with the increasing values of MPC03^{C} and HATSs^{A} the descending trend of $S_e$is observed (Fig. 5).

Influence of ion structure of ionic liquids supplemented by $I^{3-}/3I^{-}$ and $Co^{3+/2+}$ $(bpy)_3$ redox couples on the Seebeck coefficient

Two different redox shuttles were taken into account: the $I_3^{-}/3I^{-}$ and the $Co^{3+/2+}$ $(bpy)_3$. The concentration of the former system was equal to 0.01 mol/l and 0.2 mol/l, while in the cobalt redox couple case the concentration was equal to 0.01 mol/l. The two redox systems have compelling structure differences which should first be discussed. Namely, the iodine/iodide structures are significantly different to the corresponding $Co^{3+/}Co^{2+}$: cobalt complexes are relatively much larger and their charges before and after the redox process remain positive, while the $I_3^{-}/3I^{-}$ redox couples are much smaller and are always negatively charged. What is common, is the similar value of the standard redox potential, (for $I_3^{-}/3I^{-}$ and for $Co^{3+/2+}$ $(bpy)_3$ soluted in water

Table 4
MPC03^{C} values for selected ILs cations.

Cation's structure	IL10	IL 13	IL15	IL16
MPC03^{C}	2.639	2.485	1.792	1.099

Table 5
HATSs[A] values for selected ILs' anions.

Anion's structure	IL1	IL3	IL11	IL13	IL17
HATSs[A]	576.00	459.85	428.81	415.07	88.79

Both the molecule size and its branching coded by the MPC03[C] and the impact of electronegative atoms on the shape of the anions of ionic liquids, coded in the HATSa[A] descriptor are the key properties influencing the Seebeck coefficient of ionic liquids supplemented by the cobalt III/II complex salts.

values of standard redox potential amount about 0.5 V) and in both cases redox reactions are easy reversible. It is well-known that ligands present in complexes structures influence redox potentials, however only within some minor domain. Moreover, the cobalt III complex after the reduction still remains the cobalt complex, while the iodine after the reduction comes apart into 3 iodide ions. What is also interesting is the fact that iodine systems can be engaged in the formation of polyiodide chains, however the formation of this kind of chains was observed under special circumstances [72].

As it was noticed [10], in the case of 0.01 M concentrations of the $I_3^-/3I^-$ redox couple in ILs, high S_e was promoted by ILs composed of small, unsymmetrical and not branched cations and anions which exhibit high vertical electron-binding energy. This parameter is related to ionization energy. High ionization energy is related to stable, resistant anions. Actually, the anions of ILs frequently have superhalogen properties and remain very stable. In the case of the 0.01 M concentration of the $Co^{3+/2+}(bpy)_3$ redox couple in ILs, higher S_e was observed for small, unsymmetrical and not branched cations and for anions which display low electronegativity, see Fig. 6.

Consequently, we took into account the structures of 15,000 ionic liquids obtained by crossing the most popular 200 different cations and 75 anions. The S_e values were estimated by using the above-mentioned three different QSPR models, see Table 2. For the analysis we considered all ionic liquids structures, while the structures located not beyond the AD were flagged, see table S2.2 in the SI2. The Se values for structures from outside of the AD were found by extrapolating the model and could be taken into account as an estimation. It reveals that in general Seebeck coefficients for the case of soluted $Co^{3+/2+}$redox couple remain higher in comparison to the same ILs with the $I_3^-/3I^-$ system soluted there, see Fig. 7. This finding is in line with the previous studies, according to which the high S_e in $Co^{3+/2+}$ redox couple is the reason of the high-to-low electronic spin state transition. In consequence, the total entropy change gains an additional electronic component [30].

Next, we selected 450 ILs (45 cations from all of six cation groups differing in length of side chains, functional group and presence of the hydroxyl group or aromatic ring, with 10 most frequently used anions) from the virtual library of 15,000 ILs. The structures of 450 ionic liquids were the most diversified. Within this collection, the S_e values obtained the for case of the $Co^{3+/2+}$ redox couple applied were higher than the Seebeck coefficients estimated for the case of the soluted $I_3^-/3I^-$ redox salt. Moreover, we found that the S_e values in the two concentrations of $I_3^-/3I^-$ were nearly at the same level. Taking into account different aspects of cations structures, one can observe detectable regularities (but not only structural features influence the Seebeck, as it has been demonstrated above). It can be noticed that increasing the length of a carbon side chain leads to the decrease of the S_e. Such trend was observed in all groups of cations, but the most noticeable decrease of S_e was within the ammonium (IL13-IL15 ILs on Fig. 8), the phosphonium (IL23- IL24 ILs on Fig. 8), and the sulfonium (IL41, IL43 ILs on Fig. 8) ILs, where the core of the cations was composed of one central atom. The branching of the core of ILs' cations influences the S_e values too. We have noticed that the presence of an additional functional group in the core of the cation decreases the S_e values independently of the type and concentration of the redox couple used (e.g. the noticed trends in the imidazolium cations IL1, IL4, IL5 and IL8; the ammonium IL13, IL16, IL18; the phosphonium IL23, IL25, IL26, IL27 and the piridinium IL30, IL32, IL33). Furthermore, the presence of the substituent containing an aromatic ring significantly decreases the S_e. This statement is noticeable when one compares the imidazolium cations: IL1 and IL7, as well as the ammonium cations: IL16 and IL20.

Additionally, the hydroxy or alcoxy substituents present in the core of the cation do not influence the S_e values – for imidazolium ILs: IL3, IL9 and IL10; piridinium ILs: IL30 and IL35, and for pyrrolidinium ILs: IL36, IL39 and IL40 the S_e within the particular group remains the same. In the case of the carboxyl group, any change in the S_e was visible only in the presence of a long alkyl chain: imidazolium ILs: IL5, IL11, see Fig. 8. The impact of the anion structure on this dataset is also noticeable. In the presence of the $I3^-/3I^-$ redox salt the smallest S_e values (0–0.7 mV/K) were observed for the ILs containing anions characterized by low vertical electron binding energy (e.g. acetate, bromide, formate,

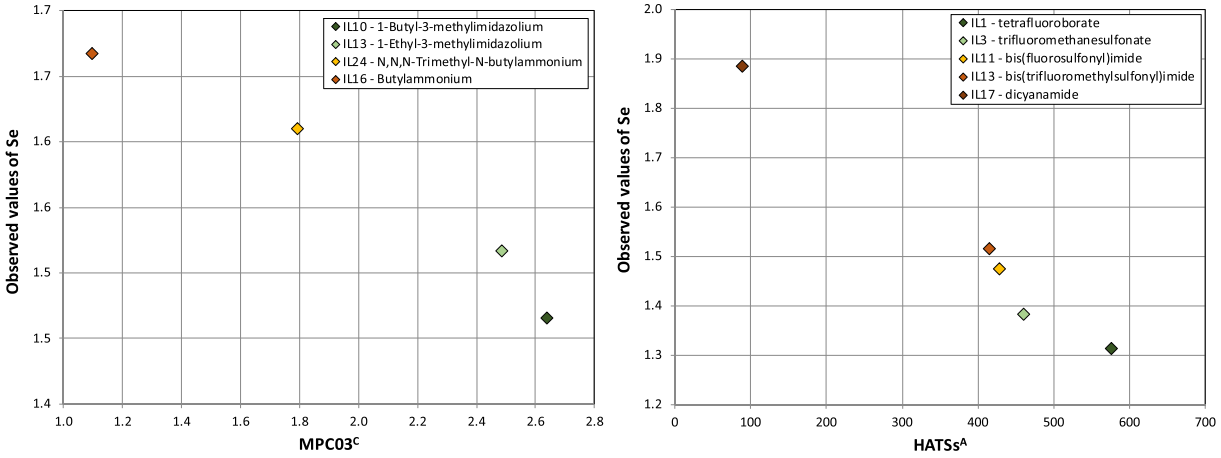

Fig. 5. Relationship between ILs' Seebeck coefficient and descriptors: left panel – MPC03[C] – ILs with a different cation, and the same anion (bis(trifluoromethanesulfonyl)imide), right panel - HATSs[A] – ILs with the same cation (1-ethyl-3-methylimidazolium) and different anions.

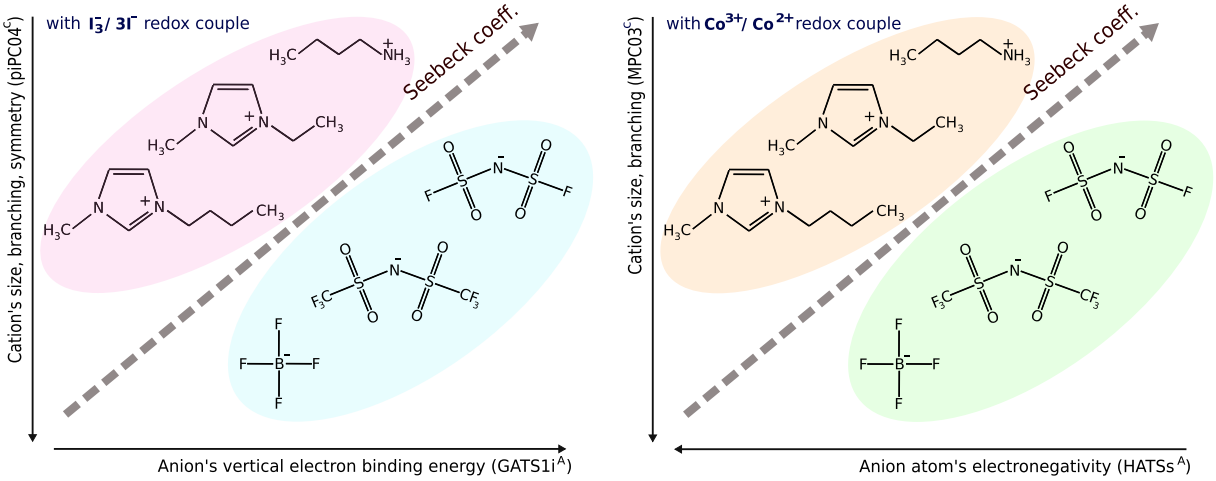

Fig. 6. Relationship between cation and anion structures and Seebeck coefficients.

nitrate). The increase of that energy discovered for anions caused the increase of the S_e values up to even 1 mV/K for ILs containing hexafluorophosphate and tetrafluoroborate. The opposite trend was observed in presence of the $Co^{3+/2+}$ redox couple. Ionic liquids containing less elctronegative anions display the highest values of the S_e (up to 2 mV/K) independently of the cation structure. The presence of hexafluorophosphate and tetrafluoroborate anions caused the decrease of the S_e up to 1.5 mV/K. It is worth noticing that even though the S_e for

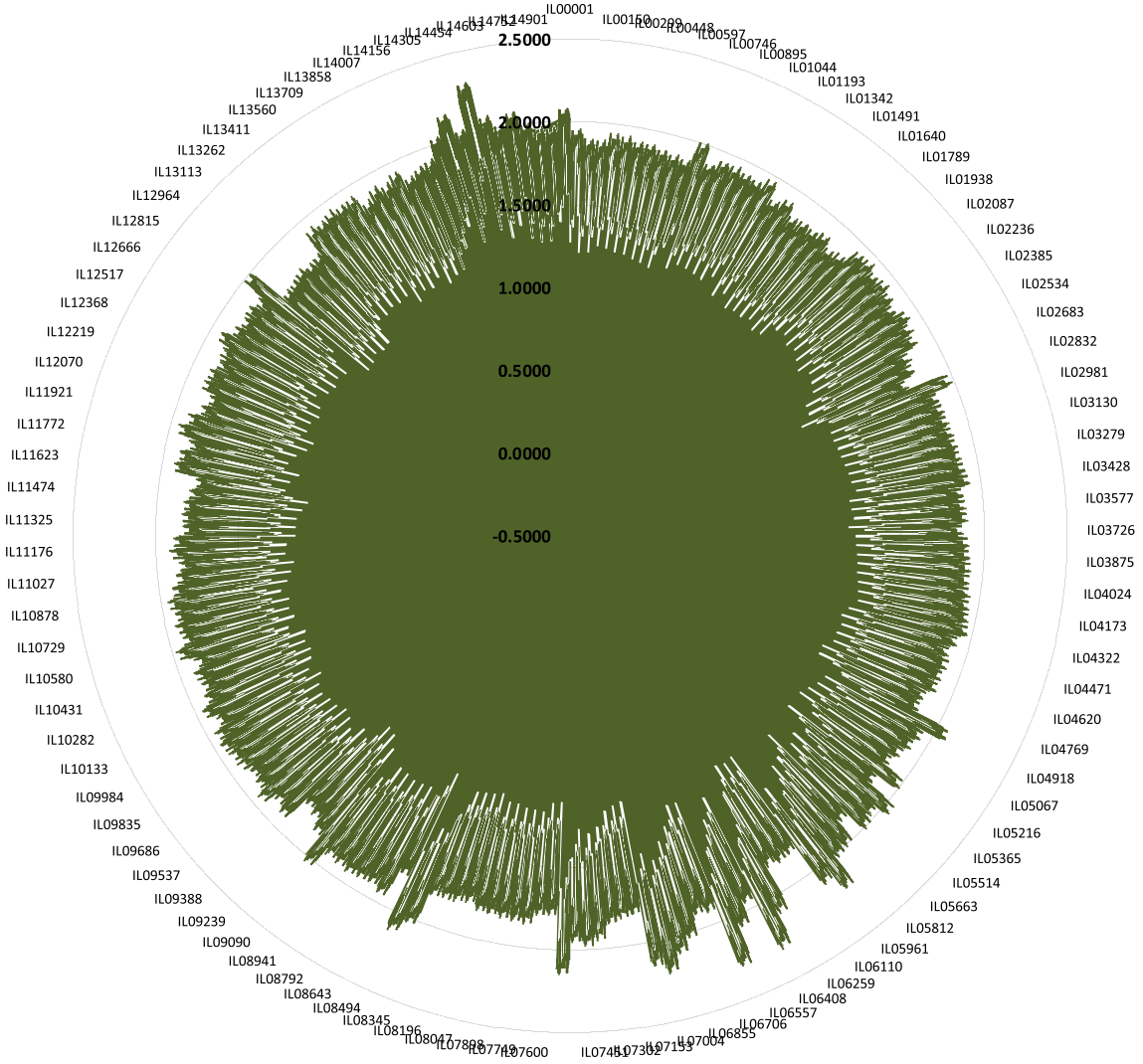

Fig. 7. The S_e values [mV/K] predicted by QSPR models: green line indicates S_e values for the case of the $Co^{2+/3+}$ redox couple, blue and orange lines indicate Seebeck coefficient values for cases of the $I_3^-/3I^-$redox couple (0.01 M and 0.2 M respectively).

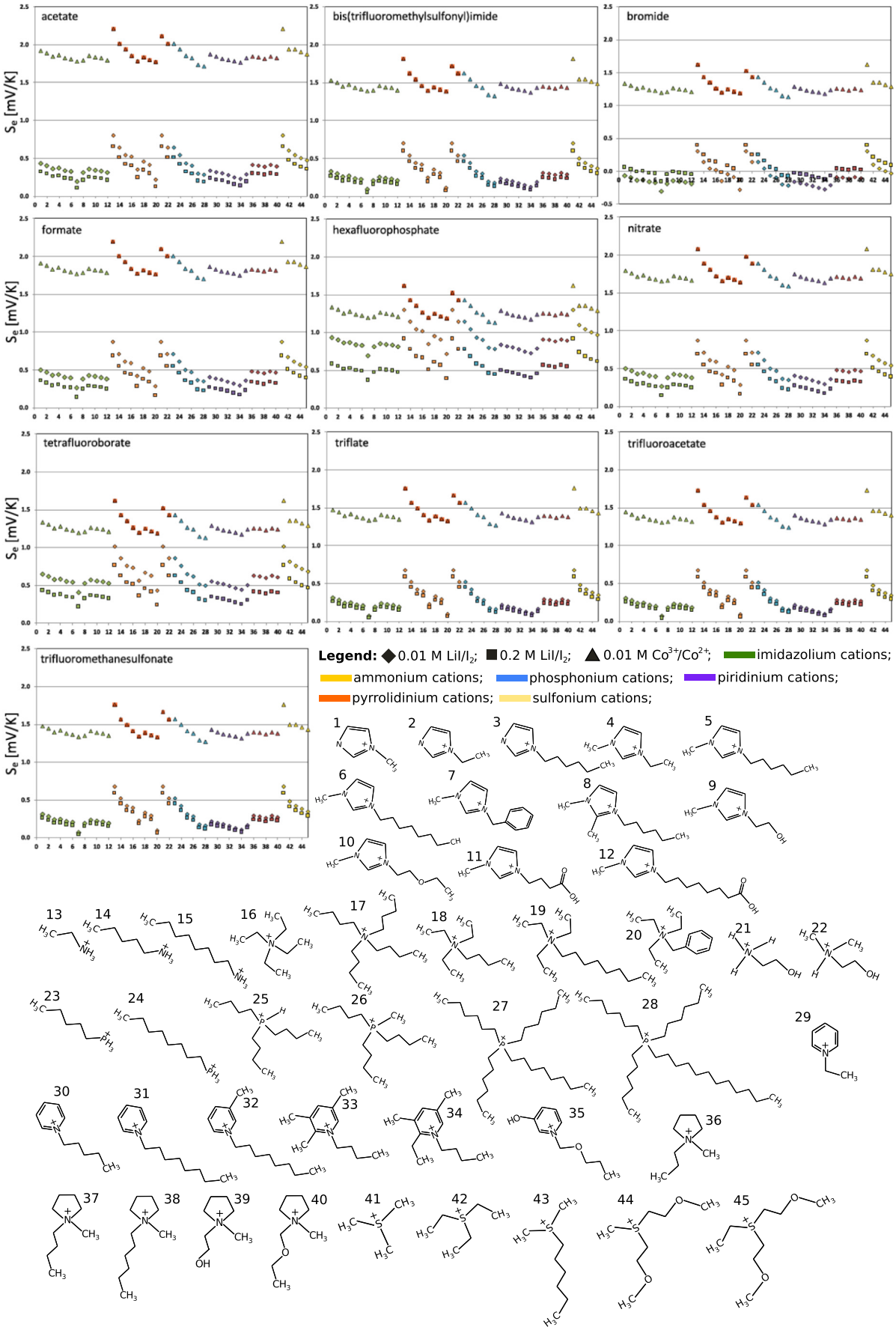

Fig. 8. Influence of structural features of ILs on the Se coefficient for 2 different redox couples for 450 ILs. Each diagram was marked with an anion of appropriate ILs for which the Seebeck coeffs. were estimated.

those ILs supplemented by the $Co^{3+/2+}$ redox couple is relatively low, it is still higher than in case of respective ILs supplemented by the $I_3^-/3I^-$ redox couple.

Additionally, the hydroxy or alcoxy substituents present in the core of the cation do not influence the S_e values – for imidazolium ILs: IL3, IL9 and IL10; piridinium ILs: IL30 and IL35, and for pyrrolidinium ILs: IL36, IL39 and IL40 the level of the S_e within a particular group remains the same. In the case of the carboxyl group, any change in S_e was visible only in the presence of a long alkyl chain: imidazolium ILs: IL5, IL11, see Fig. 8.

The impact of the anion structure on this dataset is also noticeable. In the presence of the $I_3^-/3I$- redox system the smallest S_e values (0–0.7 mV/K) were observed for the ILs containing anions characterized by low vertical electron binding energy (e.g. acetate, bromide, formate, nitrate). The increase of that energy in anions caused the increase of the S_e values up to even 1 mV/K for ILs with hexafluorophosphate and tetrafluoroborate. In this case, the structures of anions are very symmetrical and the highly electronegative fluorine atoms cause the population charge of the central atom to be likely smaller. The opposite trend was observed in the presence of the $Co^{3+/2+}$ redox couple. Here, the presence of less electronegative atoms leads to higher values of S_e (up to 2 mV/K) independently of the cations structure. The anions containing electronegative atoms (hexafluorophosphate and tetrafluoroborate) make the Seebeck coeff. decrease down to 1.5 mV/K. It is worth to notice that even though the S_e for those ILs in the $Co^{3+/2+}$ redox couple was relatively low, it was still higher than in case of ionic liquids supplemented by the $I_3^-/3I^-$ redox system.

4. Conclusion

We measured Seebeck coefficients for 17 ILs. The liquids were supplemented by a 0.01 mol/l concentration of the $Co^{3+/2+}(bpy)_3$ redox couple. On this basis we developed a QSPR algorithm and estimated Seebeck coefficients for 15,000 ionic liquids. We also estimated the Seebeck for the same 15,000 ionic liquids supplemented by two different concentrations, 0.01 and 0.2 mol/l, of the $I_3^-/3I^-$ redox system, whereas the respective QSPR algorithms were partially developed earlier (for 0.01 mol/mol concentration) [10]. The ILs ensemble was sufficiently large to deliver substantial conclusions. First of all, the Seebeck effect in ionic liquids has not been thoroughly investigated. Meanwhile, the mechanism based on thermodiffusion of ions from one electrode to another has been assumpted, it seems. However, it is difficult to explain the high neat ILs' Seebeck coefficient only on this basis [23]. The electrodes are certainly attached to voltometer by metal wires which transmit electrons, not ions. This means that redox reactions might occur with the participation of ILs ions, whether they were supplemented by some redox couples or not. The Seebeck coefficient is distinctly experimental property. Especially for solutions there is no general theoretical equation determining the Seebeck coefficient where electrochemical reactions were taken into account. Hence, any study pointing to the relation between the structure of ionic liquids and the corresponding Seebeck coefficient, as well as shedding some light on Seebeck effect in liquids, is valuable.

So far, it has been revealed that there is a significant dependency between the structure of ionic liquids and the Seebeck effect. A great many IL structures are achievable, with only some amount of redox couples. We found that small, symmetrical and not branched cations and anions, which contain relatively less electronegative atoms, make the Seebeck increase. The effect of anions is dependent on the redox couple system applied, and in general the highly symmetrical anions containing electronegative fluorine atoms increase the Seebeck coefficient. The highest Seebeck coefficient, exceeding 2.3 mV, was predicted for the N·N.*N*-tetramethylammonium triethyl-n-hexylboride, N-ethylammonium triethyl-n-hexylboride and for trimethylsulfonium triethyl-n-hexylboride ionic liquids. Moreover it revealed not only one ion type from the ionic liquid compound influenced the Seebeck but the combination of cation and anion played the role. We also discovered that the cobalt-based redox couples are much better than the one based on the iodine/iodide system for thermo-electric applications, however higher concentrations of cobalt can cause pollutions in the environment, while the ILs applications are sometimes called the green chemistry. We are convinced the developed QSPR algorithm for predicting Seebeck and for designing a better ionic liquid (to achieve the better Seebeck) can have an impact on the practical design of the liquid-based thermo-electric devices of a desired purpose.

References:

[1] British Petrol Statistical Review of World Energy 2019, 68th edition, Https://Www. Bp.Com/Content/Dam/Bp/Business-Sites/En/Global/Corporate/Pdfs/Energy-Eco-nomics/Statistical-Review/Bp-Stats-Review-2019-Full-Report.Pdf. (2019).
[2] Danish Energy Statistics 2016, https://ens.dk/sites/ens.dk/files/Statistik/energy 2016.
[3] Energy Efficiency, 2009. European Comission, 2009, http://prtr-es.es/Data/images//Eficiendia-energ%C3.
[4] E. Laux, S. Uhl, T. Journot, J. Brossard, L. Jeandupeux, H. Keppner, Aspects of protonic ionic liquid as electrolyte in thermoelectric generators, J. Electron. Mater. 45 (2016) 3383–3389, https://doi.org/10.1007/s11664-016-4526-1.
[5] M. Palacio, B. Bhushan, A review of ionic liquids for green molecular lubrication in nanotechnology, Tribol. Lett. 40 (2010) 247–268, https://doi.org/10.1007/s11249-010-9671-8.
[6] S. Keskin, D. Kayrak-Talay, U. Akman, Ö. Hortaçsu, A review of ionic liquids towards supercritical fluid applications, J. Supercrit. Fluids 43 (2007) 150–180, https://doi. org/10.1016/j.supflu.2007.05.013.
[7] D.R. Macfarlane, M. Forsyth, P.C. Howlett, J.M. Pringle, J. Sun, G. Annat, W. Neil, E.I. Izgorodina, Ionic liquids in electrochemical devices and processes: managing inter-facial electrochemistry, Acc. Chem. Res. 40 (2007) 1165–1173, https://doi.org/10. 1021/ar7000952.
[8] P. Wasserscheid, W. Keim, Ionic liquids—new "solutions" for transition metal catal-ysis, Angew. Chem. 39 (2002) 3772–3789, https://doi.org/10.1002/1521-3773 (20001103)39:21<3772::aid-anie3772>3.0.co;2-5.
[9] T. Welton, Room-temperature ionic liquids. Solvents for synthesis and catalysis, Chem. Rev. 99 (1999) 2071–2084, http://www.ncbi.nlm.nih.gov/pubmed/11849019.
[10] A. Sosnowska, M. Barycki, A. Gajewicz, M. Bobrowski, S. Freza, P. Skurski, S. Uhl, E. Laux, T. Journot, L. Jeandupeux, H. Keppner, T. Puzyn, Towards the application of structure–property relationship modeling in materials science: predicting the Seebeck coefficient for ionic liquid/redox couple systems, ChemPhysChem 17 (2016) 1591–1600, https://doi.org/10.1002/cphc.201600080.
[11] M.J. Earle, K.R. Seddon, Ionic liquids. Green solvents for the future, Pure Appl. Chem. 72 (2007) 1391–1398, https://doi.org/10.1351/pac200072071391.
[12] E.W. Castner, J.F. Wishart, Spotlight on ionic liquids, J. Chem. Phys. 132 (2010) 120901–120909, https://doi.org/10.1063/1.3373178.
[13] F. Endres, O. Höfft, N. Borisenko, L.H. Gasparotto, A. Prowald, R. Al-Salman, T. Carstens, R. Atkin, A. Bund, S. Zein El Abedin, Do solvation layers of ionic liquids in-fluence electrochemical reactions? Phys. Chem. Chem. Phys. 12 (2010) 1724–1732, https://doi.org/10.1039/b923527m.
[14] H.-O. Hamaguchi, R. Ozawa, Structure of ionic liquids and ionic liquid compounds: are ionic liquids genuine liquids in the conventional sense? ChemInform 36 (2005), https://doi.org/10.1002/chin.200547277.
[15] H. Weingärtner, Understanding ionic liquids at the molecular level: facts, problems, and controversies, Angew. Chem. Int. Ed. 47 (2008) 654–670, https://doi.org/10. 1002/anie.200604951.
[16] M.G. Del Pópolo, G.A. Voth, On the structure and dynamics of ionic liquids, J. Phys. Chem. B 108 (2004) 1744–1752, https://doi.org/10.1021/jp0364699.
[17] J.N.A. Canongia Lopes, A.A.H. Pádua, Nanostructural organization in ionic liquids, J. Phys. Chem. B 110 (2006) 3330–3335, https://doi.org/10.1021/jp056006y.
[18] R. Atkin, G.G. Warr, The smallest amphiphiles: nanostructure in protic room-temperature ionic liquids with short alkyl groups, J. Phys. Chem. B 112 (2008) 4164–4166, https://doi.org/10.1021/jp801190u.
[19] A. Triolo, O. Russina, H.J. Bleif, E. Di Cola, Nanoscale segregation in room temperature ionic liquids, J. Phys. Chem. B 111 (2007) 4641–4644, https://doi.org/10.1021/jp067705t.
[20] C. Chiappe, D. Pieraccini, Ionic liquids: solvent properties and organic reactivity, J. Phys. Org. Chem. 18 (2005) 275–297, https://doi.org/10.1002/poc.863.
[21] M. Freemantle, Designer solvents: ionic liquids may boost clean technology devel-opment, Chem. Eng. News 76 (1998) 32–37, https://doi.org/10.1021/cen-v076n013.p032.
[22] A.R. Katritzky, R. Jain, A. Lomaka, R. Petrukhin, M. Karelson, A.E. Visser, R.D. Rogers, Correlation of the melting points of potential ionic liquids (imidazolium bromides and benzimidazolium bromides) using the CODESSA program, J. Chem. Inf. Comput. Sci. 42 (2002) 225–231, https://doi.org/10.1021/ci0100494.
[23] H. Jia, X. Tao, Y. Wang, Flexible and self-healing thermoelectric converters based on thermosensitive liquids at low temperature gradient, Advanced Electronic Mate-rials. 2 (2016) 1600136(1)–1600136(7), https://doi.org/10.1002/aelm.201600136.
[24] H. Jia, Z. Ju, X. Tao, X. Yao, Y. Wang, P-N conversion in a water-ionic liquid binary system for nonredox thermocapacitive converters, Langmuir 33 (2017) 7600–7605, https://doi.org/10.1021/acs.langmuir.7b00746.
[25] M. Bonetti, S. Nakamae, M. Roger, P. Guenoun, Huge Seebeck coefficients in non-aqueous electrolytes, J. Chem. Phys. 134 (2011) 114513–1–114513–114518, https://doi.org/10.1063/1.3561735.
[26] B.T. Huang, M. Roger, M. Bonetti, T.J. Salez, C. Wiertel-Gasquet, E. Dubois, R. Cabreira Gomes, G. Demouchy, G. Mériguet, V. Peyre, M. Kouyaté, C.L. Filomeno, J. Depeyrot, F.A. Tourinho, R. Perzynski, S. Nakamae, Thermoelectricity and thermodiffusion in charged colloids, J. Chem. Phys. (2015), https://doi.org/10.1063/1.4927665.
[27] E. Laux, S. Uhl, L. Jeandupeux, P.P. López, P. Sanglard, E. Vanoli, R. Marti, H. Keppner, Thermoelectric generators based on ionic liquids, J. Electron. Mater. 47 (2018) 3193–3197, https://doi.org/10.1007/s11664-018-6175-z.
[28] E. Laux, S. Uhl, N. Gauthier, L. Jeandupeux, H. Keppner, P.P. López, S. Pauline, E. Vanoli, R. Marti, Development of thermoelectric generator based on ionic liquids for high temperature applications, Materials Today: Proceedings. 5 (2018) 10195–10202, https://doi.org/10.1016/j.matpr.2017.12.265.
[29] M. Barycki, A. Sosnowska, A. Gajewicz, M. Bobrowski, D. Wileńska, P. Skurski, A. Giełdoń, C. Czaplewski, S. Uhl, E. Laux, T. Journot, L. Jeandupeux, H. Keppner, T. Puzyn, Temperature-dependent structure-property modeling of viscosity for ionic liquids, Fluid Phase Equilib. 427 (2016) 9–17, https://doi.org/10.1016/j.fluid.2016. 06.043.
[30] D. Al-Masri, M. Dupont, R. Yunis, D.R. MacFarlane, J.M. Pringle, The electrochemistry and performance of cobalt-based redox couples for thermoelectrochemical cells, Electrochim. Acta 269 (2018) 714–723, https://doi.org/10.1016/j.electacta.2018.03. 032.
[31] T.J. Abraham, D.R. MacFarlane, J.M. Pringle, Seebeck coefficients in ionic liquids -prospects for thermo-electrochemical cells, Chem. Commun. 47 (2011) 6260–6262, https://doi.org/10.1039/C1cc11501d.
[32] J. He, D. Al-Masri, D.R. MacFarlane, J.M. Pringle, Temperature dependence of the electrode potential of a cobalt-based redox couple in ionic liquid electrolytes for thermal energy harvesting, Faraday Discuss. 190 (2016) 205–218, https://doi.org/ 10.1039/c5fd00238a.
[33] J.H. Yum, E. Baranoff, F. Kessler, T. Moehl, S. Ahmad, T. Bessho, A. Marchioro, E. Ghadiri, J.E. Moser, C. Yi, M.K. Nazeeruddin, M. Grätzel, A cobalt complex redox shuttle for dye-sensitized solar cells with high open-circuit potentials, Nat. Commun. 631 (2012), https://doi.org/10.1038/ncomms1655.
[34] G. Sliwoski, S. Kothiwale, J. Meiler, E. W. Lowe, Jr., Computational methods in drug discovery, Pharmacol. Rev. 66 (2014) 334–395.
[35] S.P. Leelananda, S. Lindert, Computational methods in drug discovery, Beilstein J. Org. Chem. 12 (2016) 2694–2718, https://doi.org/10.3762/bjoc.12.267.
[36] S. Hammes-Schiffer, Catalysts by design: the power of theory, Acc. Chem. Res. 50 (2017) 561–566, https://doi.org/10.1021/acs.accounts.6b00555.
[37] A. Mikolajczyk, A. Gajewicz, E. Mulkiewicz, B. Rasulev, M. Marchelek, M. Diak, S. Hirano, A. Zaleska-Medynska, T. Puzyn, Nano-QSAR modeling for ecosafe design of heterogeneous TiO 2 -based nano-photocatalysts, Environ. Sci. Nano 5 (2018) 1150–1160, https://doi.org/10.1039/c8en00085a.
[38] M. Barycki, A. Sosnowska, T. Puzyn, AquaBoxIL-a computational tool for determining the environmental distribution profile of ionic liquids, Green Chem. 20 (2018) 3359–3370, https://doi.org/10.1039/c8gc01582a.
[39] E. Wyrzykowska, A. Rybińska-Fryca, A. Sosnowska, T. Puzyn, Virtual screening in the design of ionic liquids as environmentally safe bactericides, Green Chem. 21 (2019) 1965–1973, https://doi.org/10.1039/c8gc03400a.
[40] A. Rybinska, A. Sosnowska, M. Grzonkowska, M. Barycki, T. Puzyn, Filling environ-mental data gaps with QSPR for ionic liquids: modeling n-octanol/water coefficient, J. Hazard. Mater. 303 (2016) 137–144, https://doi.org/10.1016/j.jhazmat.2015.10. 023.
[41] A. Rybinska, A. Sosnowska, M. Barycki, T. Puzyn, Geometry optimization method versus predictive ability in QSPR modeling for ionic liquids, J. Comput. Aided Mol. Des. 30 (2016) 165–176.
[42] K. Jagiello, A. Sosnowska, S. Kar, S. Demkowicz, M. Daśko, J. Leszczynski, J. Rachon, T. Puzyn, Geometry optimization of steroid sulfatase inhibitors - the influence on the free binding energy with STS, Struct. Chem. 28 (2017) 1017–1032, https://doi.org/ 10.1007/s11224-016-0903-x.
[43] R.N. Das, K. Roy, P.L.A. Popelier, Exploring simple, transparent, interpretable and predictive QSAR models for classification and quantitative prediction of rat toxicity of ionic liquids using OECD recommended guidelines, Chemosphere 139 (2015) 163–173, https://doi.org/10.1016/j.chemosphere.2015.06.022.

[44] K. Roy, R.N. Das, P.L.A. Popelier, Predictive QSAR modelling of algal toxicity of ionic liquids and its interspecies correlation with Daphnia toxicity, Environ. Sci. Pollut. Res. 22 (2015) 6634–6641, https://doi.org/10.1007/s11356-014-3845-0.
[45] M. Barycki, A. Sosnowska, T. Puzyn, Which structural features stand behind micelization of ionic liquids? Quantitative structure-property relationship studies, J. Colloid Interface Sci. 487 (2017) 475–483, https://doi.org/10.1016/j.jcis.2016.10. 066.
[46] Version 11. 0. ACD/ChemSketch Advanced Chemistry Development, Inc., Toronto, ON, Canada, www.acdlabs.com, No Title, (2008).
[47] J.J.P. Steward, Optimization of parameters for semiempirical methods V:modification of NDDO approximations and application to 70 elements, J. Mol. Model. 13 (2007) 1173–1213.
[48] T.J. Abraham, D.R. MacFarlane, J.M. Pringle, High Seebeck coefficient redox ionic liq-uid electrolytes for thermal energy harvesting, Energy Environ. Sci. 6 (2013) 2639–2645, https://doi.org/10.1039/C3EE41608A.
[49] M.J.J.P. Stewart, Stewart Computational Chemistry, Colorado Springs, CO, USA, 2012.
[50] Talete, Dragon, Software for Molecular Descriptor Calculation, http://www.talete.mit/ 2014.
[51] C.M. R. Andersen Bro, Variable selection in regression - a tutorial, J. Cheminform. 24 (2010) 728–737
[52] P. Gramatica, N. Chirico, E. Papa, S. Cassani, S. Kovarich, QSARINS: a new software for the development, analysis, and validation of QSAR MLR models, J. Comput. Chem. 34 (2013) 2121–2132, https://doi.org/10.1002/jcc.23361.
[53] S. P. Gramatica Cassani, N. Chirico, J. Comput. Chem. 35 (2014) 1036–1044 (QSARINS-chem: Insubria datasets and new QSAR/QSPR models for environmental pollutants in QSARINS, Journal of Computational Chemistry, 35 (2014) 1036–1044)
[54] M.T.D. Cronin, T.W. Schultz, Pitfalls in QSAR, J. Mol. Struct. Theochem. 622 (2003) 39–51, doi: Pii S0166-1280(02)00616-4, https://doi.org/10.1016/S0166-1280(02) 00616-4.
[55] T.W. Schultz, M.T.D. Cronin, T.I. Netzeva, The present status of QSAR in toxicology, J. Mol. Struct. THEOCHEM 622 (2003) 23–38.
[56] A. Tropsha, P. Gramatica, V.K. Gombar, The importance of being earnest: validation is the absolute essential for successful application and interpretation of QSPR models, QSAR Comb. Sci. 22 (2003) 69–77.
[57] P. Gramatica, P. Pilutti, E. Papa, Validated QSAR prediction of OH tropospheric deg-radation of VOCs: splitting into training-test sets and consensus modeling, J. Chem. Inf. Comput. Sci. 44 (2004) 1794–1802, https://doi.org/10.1021/ci049923u.
[58] T. Puzyn, A. Mostrag-Szlichtyng, A. Gajewicz, M. Skrzyński, A.P. Worth, Investigating the influence of data splitting on the predictive ability of QSAR/QSPR models, Struct. Chem. 22 (2011) 795–804, https://doi.org/10.1007/s11224-011-9757-4.
[59] N. Chirico, P. Gramatica, Real external predictivity of QSAR models. Part 2. New intercomparable thresholds for different validation criteria and the need for scatter plot inspection, J. Chem. Inf. Model. 52 (2012) 2044–2058, https://doi.org/10.1021/ci300084j.
[60] P.K. Ojha, I. Mitra, R.N. Das, K. Roy, Further exploring r(m)(2) metrics for validation of QSPR models, Chemom. Intell. Lab. Syst. 107 (2011) 194–205, https://doi.org/10. 1016/j.chemolab.2011.03.011.
[61] K. Roy, R.N. Das, P. Ambure, R.B. Aher, Be aware of error measures. Further studies on validation of predictive QSAR models, Chemom. Intell. Lab. Syst. 152 (2016) 18–33, https://doi.org/10.1016/j.chemolab.2016.01.008.
[62] D.L.J. Alexander, A. Tropsha, D.A. Winkler, Beware of R-2: simple, unambiguous assessment of the prediction accuracy of QSAR and QSPR models, J. Chem. Inf. Model. 55 (2015) 1316–1322.
[63] N. Chirico, P. Gramatica, Real external predictivity of QSAR models: how to evaluate it? Comparison of different validation criteria and proposal of using the concordance correlation coefficient, J. Chem. Inf. Model. 51 (2011) 2320–2335, https://doi.org/10. 1021/ci200211n.
[64] A. Tropsha, Best practices for QSAR model development, validation, and exploita-tion, Molecular Informatics 29 (2010) 476–488, https://doi.org/10.1002/minf. 201000061.
[65] K. Roy, P. Ambure, The "double cross-validation" software tool for MLR QSAR model development, Chemom. Intell. Lab. Syst. 159 (2016) 108–126.
[66] S. Wold, L. Eriksson, Statistical Validation of QSAR Results. Weinheim, 1995.
[67] S. Zhang, A. Golbraikh, S. Oloff, K. H., A novel automated lazy learning QSAR (ALL-QSAR) approach: method development, applications, and virtual screening of chemical databases using validated ALL, J. Mol. Graph. Model. 46 (2006) 1984–1995.
[68] A. Tropsha, P. Gramatica, V.K. Gombar, The importance of being earnest: validation is the absolute essential for successful application and interpretation of QSPR models, QSAR Comb. Sci. 22 (2003) 69–77.
[69] J. Jaworska, N. Nikolova-Jeliazkova, T. Aldenberg, QSAR applicability domain estima-tion by projection of the training set in descriptor space: a review, ATLA 33 (2005) 445–459.
[70] V. R. Todescini Consonni, Handbook Od Molecular Descriptors, WILEY-VCH, Weinheim, 2000.
[71] L.H. Hall, L.B. Kier, Electrotopological state indexes for atom types - a novel combi-nation of electronic, topological, and valence state information, J. Chem. Inf. Comput. Sci. 35 (1995) 1039–1045.
[72] S. Madhu, H.A. Evans, V.V.T. Doan-Nguyen, J.G. Labram, G. Wu, M.L. Chabinyc, R. Seshadri, F. Wudl, Infinite polyiodide chains in the pyrroloperylene—iodine com-plex: insights into the starch—iodine and Perylene—iodine complexes, Angew. Chem. Int. Ed. (2016), https://doi.org/10.1002/anie.201601585.